THE QUEBEC LONG FLUME: HYDRAULIC DESIGN AND CALIBRATION OF A NEW VERSATILE LARGE FLUME

Bernard Long[1], Régis Xhardé[1], Mathieu Desroches[1]

Abstract

The aim of this paper is to report a new and unique facility, the Quebec long flume (QLF), which offers a wide range of hydrodynamic conditions to study a large variety of coastal processes. Hydraulic design details of the QLF are presented and preliminary results of the first set of hydraulic calibration experiments are discussed. Acoustic Doppler Velocimeters (ADV) measurements reveal the presence of a significant return flow in the water column under sine wave conditions. Results indicate that the flow is oriented in the opposite direction of wave propagation, with mean horizontal velocities ranging between -4 cm/s and -30 cm/s depending on the wave height. Floor-induced turbulence is limited to a 1.7 cm thick layer above the floor. Water level was also recorded by water gages and compared with the theoretical simulated wave shape (Airy wave or sine wave). Results show that the wave shape is altered by bed friction for long wave periods ($T \geq 6$ s) and tends to a cnoidal shape with steeper crests and flatter troughs. These findings will allow correcting systematic flume-induced biases and will lead to more accurate measurements in forthcoming hydraulics experiments.

Key words: hydrodynamics, hydraulics, flume, calibration, wave.

1. Introduction

Although a lot of progress concerning mathematical and numerical modeling was made in recent decades, physical models, especially large-scale models, are still important for investigations in coastal engineering. Analytical studies are unable to describe accurately non-linear processes such as wave breaking, turbulent currents, or the complex interactions between waves, sediments and structures in the surf zone (Dette et al., 2002). Field measurements are extremely expensive and time-consuming, and the interpretation of results is very difficult due to a large number of overlapping influences. Investigations in small-scale models are affected by scale effects resulting from the inability to satisfy the laws of similitude (Kamphuis, 1974; Hudson et al., 1979; Dalrymple, 1989; Hughes, 1993; Heller, 2011). In particular, scaling of beach material in movable-bed models is often impossible (Kamphuis, 1974; Hudson et al., 1979). All these disadvantages are considerably reduced when a large-scale facility is used for testing a wide range of interactions between wave parameters and coastal morphology. The large flumes enable the acquisition of data from controlled experiments at a scale close to the real-world prototype to study the processes as well as to verify or calibrate numerical models for prediction about beach evolution, sediment transport or coastal structure response to storms and waves. The aim of this paper is to report a new and unique facility, the Quebec long flume from the environmental hydraulic laboratory, which offers a wide range of hydrodynamic conditions to study a large variety of coastal processes. First, the design and parameters of the flume are presented. Then, the preliminary results of the first set of hydraulic measurements are discussed.

2. The Quebec Long Flume (QLF) Laboratory

The QLF is a 120 m long outdoor flume with a rectangular cross-section of 5x5 m located in Quebec City, Canada. It was built in 2011 by the National Institute of Scientific Research (INRS-ETE). The main parameters of the flume are presented in Table 1. The flume bed and walls are made of reinforced concrete and lies on the bedrock to avoid flume deformation.

[1]INRS-ETE, University of Quebec, 490 rue de la Couronne, Québec, G1K 9A9, Canada. blong@ete.inrs.ca

Table 1. Main technical characteristics of the Quebec Long Flume.

Length	120 m
Width	5.0 m
Height of walls	5.0 m
Max. water depth	3.9 m
Min. water depth	2.0 m
Flow rate	5 m³/s
Wave type	Airy, cnoidal, Stokes, solitary
Wave period	from 0.5 s to 12 s
Wave height	from 0.01 m to 1.8 m
Working regime	Wave, tide, current

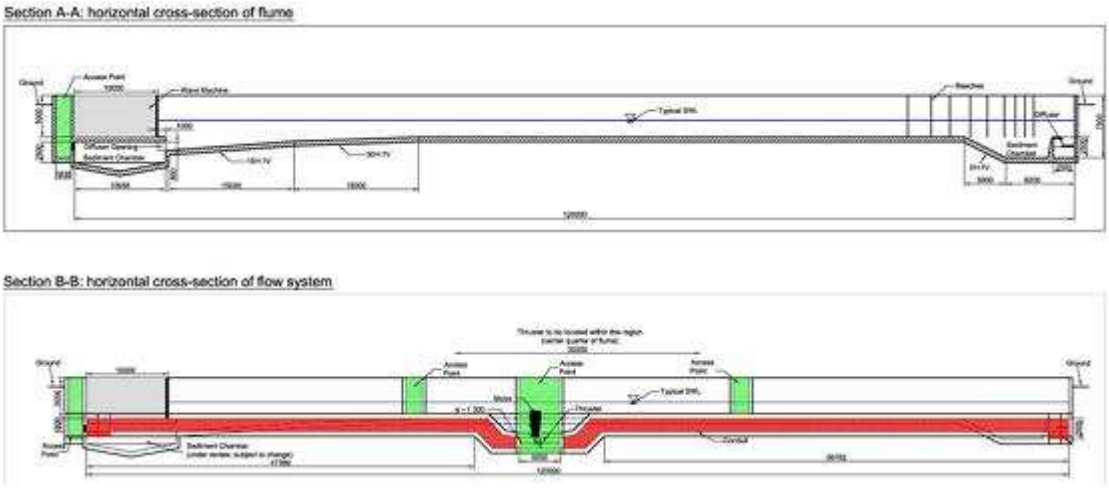

Figure 1. Schematic view of the hydraulic flume of the National Institute of Scientific Research (INRS-ETE).

At the downstream end of the flume, a riprap made of granitic blocks weighting between 200 kg and 400 kg was installed with a slope of 1/6 to absorb wave energy and avoid wave reflection. The attenuation coefficient of this structure is estimated between 90 % and 92 %. A linear water tank with a capacity of about 3300 m³ is located parallel to the flume (Fig. 1, section A-A').

The QLF is equipped with a MTS wave maker entirely operated by computer. The wave maker is controlled by two wave gage transducers and one active wave absorber allowing an accurate control of the wave characteristics (i.e. height and period). Four main types of wave can be generated in the QLF: Airy wave (sine wave), cnoidal wave, Stokes wave under the approximations of Pierson-Moskowitz (Pierson and Moskowitz, 1964), JONSWAP (Hasselmann et al., 1976) and Ochi-Hubble (Ochi and Hubble, 1976), and solitary wave (tsunami). Wave period can range from 0.5 s to 12 s and wave height can be set from 0.01 m to a maximum wave height of 1.80 m. The power of the wave maker can be adjusted in function of the water level within the flume in order to generate waves in water depth ranging from 2.0 m to 3.9 m.

The flume is also equipped with a Flygt NZ horizontal pump from ITT Water & Wastewater for the filling and draining operations. The maximum discharge rate is 0.55 m³/s and the effective discharge rate is 0.40 m³/s, allowing the complete drainage of the flume in about 150 minutes. The pump system can also be used simultaneously with the wave maker to simulate the combined effects of wave and tide. Moreover, a bidirectional water circulation system can be created in the flume using a Rolls-Royce/Kamewa Ulstein tunnel thruster (Fig. 1, section B-B'). The thruster power ranges from 350 kW to 590 kW and is able to generate a 1 m/s current in 1 m depth of water (equivalent to a 5 m³/s flood). Furthermore, the flow can be reversed to simulate tide reversal. The current diffuser is 1 m high and 5 m wide and is located just below the wave maker to ensure a uniform flow on the entire width of the flume.

In summary, depending on experimental design, the flume can be run using 3 main working regimes: wave-only, tide-only and current-only, or any combination of these three regimes (wave and tide; wave, tide and current; wave and current or tide and current). The wave height, wave period, water depth and flow rate are fully adjustable to allow a wide range of hydrodynamic conditions and to ensure a large diversity of Froude and Reynolds numbers. Sediment type and bed slope can also be adjusted to fit to a wide range of coastlines, from sandy beaches to cobble beaches, with reduced scale effects. To our knowledge, all these features make the QLF a unique facility to study the complexity of coastal hydrodynamics processes.

2.1. *Monitoring Equipment*

The flume is equipped with rails along the top of each wall to support and guide a 10 ton gantry crane and a mobile platform which can take a large variety of instruments. Currently, the mobile platform is equipped with a 675 MHz Imagenex multi-beam system (model Delta T 837B) and a 260 kHz Imagenex digital multi-beam imaging sonar (model 965e) for accurate bathymetry and bed morphology mapping. The platform is also equipped with an acoustic Doppler current profiler (ADCP) for current and turbulence measurement within the water column, a vertical line of five optical backscattering systems (OBS) for suspended sediment monitoring, an underwater camera, and a bed load sampler. In addition, a portable infrared (IR) laser system (MAPLE-INO) can be mounted on the platform to measure seabed laser reflectance. This laser system relies on the same principles than LiDAR systems (i.e. Krabill et al. 1995, Baltsavias 1999, Brock et al. 2002, Irish et al., 2000) and has been specifically designed by the National Institute for Optics (INO) for the INRS-ETE. Several studies conducted at the INRS-ETE have shown that the laser reflectance can be related to a number of sediment properties such as mineralogy (Long and Robitaille, 2009) and compaction (Long et al., 2010).

In addition to the mobile platform, 14 fixed equipment supports are mounted on the left side wall of the flume with a spacing of 5 m, delimiting a 65 m long test section (Fig. 2). This test section starts at 45 m from the wave maker and ends at 110 m. These 14 monitoring stations can be equipped with a variety of current meters (two Mini-ADP 3MHz from Sontek, two Aquadropp HR 2MHz from Nortek, 13 ADV Vectrino from Nortek, 4 ADV Vectrino II from Nortek, 2 ADCP Workhorse Sentinel 614kHz from RD Instruments, and 4 Electro Magnetic S4 from InterOcean), 24 turbidity sensors (OBS 3+), 30 water level sensors (15 Druck 183, and 15 Keller 169-L pressure sensors), 3 Multi Sea Cam waterproof cameras, 3 Honeywell external cameras, 17 Kyowa strain gages (model KFW 5/2) and 6 water content reflectometers (CS616 WCR). 14 RBR water level probes (model WG-50), spaced by 5 m, are also fixed on the right side wall of the flume along the test section in order to monitor the profile of the waves generated in the QLF. Table 3 summarizes all the instrumentation that can be used in the QLF.

Figure 2. View of the monitoring stations. They are located along the left wall of the flume with a spacing of 5 m and they delimit a test section of 65 m long (photo credit: Corinne Brunelle).

Table 2. Summary of the instruments that can be used in the QLF.

Instruments	Type of measure
RBR WG-50 probes	Water level
Kyowa strain gages	Water level
Electromagnetic S4	Water level, current
Acoustic Doppler current profilers	Current velocity
675 MHz Imagenex multi-beam	Bed mapping
260 kHz Imagenex digital multi-beam sonar	Bed mapping
Optical backscattering system	Turbidity
Bedload sampler	Bedload transport
Water content reflectometers	Turbidity
Multi Sea underwater camera	Bedform
Portable IR laser system (MAPLE-INO)	Sediment reflectance

Sampling monitoring, data acquisition and analog/digital signal conversion (180 channels mounted on 6 modules with 30 channels each and recording at 250 kHz) for each station is entirely controlled by a re-configurable embedded control and acquisition system from National Instruments (NI CompactRIO) operated through the graphical development environment LabVIEW. This software offers configuration-based tools and powerful programming capabilities for developing fully customized measurement, analysis, and control applications with professional user interfaces.

2.2. *Hydraulic Tests*

As with any new research facility, the flume required thorough hydraulic testing at various flow rates and regimes. Two major tests are investigated in this paper: (1) measurements of water surface profiles for a wide range of wave heights, wave periods and water depths to quantify wave profile deformation during its propagation in the flume in wave-only regime, and (2) measurements of 3-dimensional velocity vectors in various points in the water column to identify the flow structure for particular wave profile, and to quantify wall- and floor-induced turbulence in wave-only regime. The hydraulic tests were performed with 3 different wave heights (H = 0.5 m, 1.0 m, and 1.5 m), 6 different wave periods (T = 1.5 s, 2 s, 4 s, 6 s, 8 s, and 10 s) and 4 different water levels (h = 2.5 m, 3.0 m, 3.5 m and 3.9 m) for a total of 72 hydraulic tests. Data were acquired by 4 fixed monitoring stations spaced by 10 m (Fig. 3). The first one was located at 45 m from the wave maker (station 1). The three others stations were respectively located at 55 m (station 3), 65 m (station 5) and 75 m (station 7) from the wave maker.

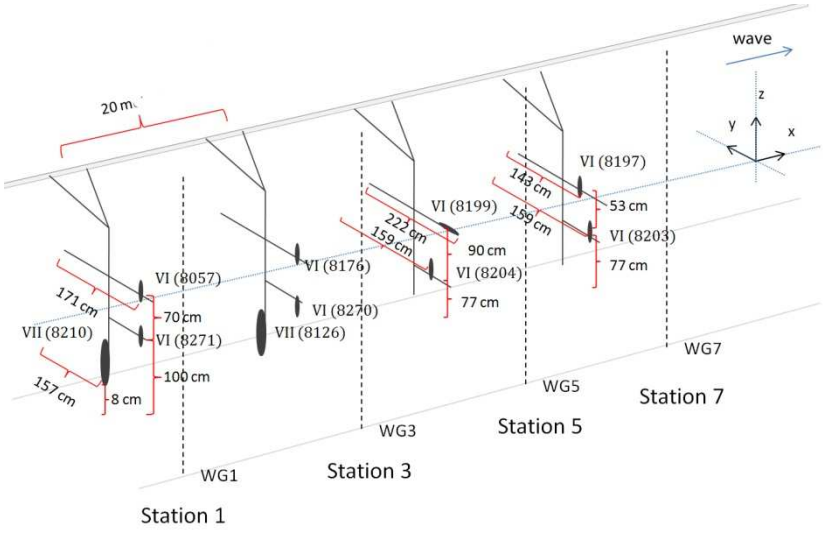

Figure 3. Experimental set-up. Four stations spaced by 10 m were equipped with 2 ADV Vectrino current meters (VI) and 2 ADV Vectrino II (VII). The latter were present only at stations 1 and 2. Water gages (WG) were positioned on the opposite wall (dotted vertical lines) to record water level fluctuations and wave shape.

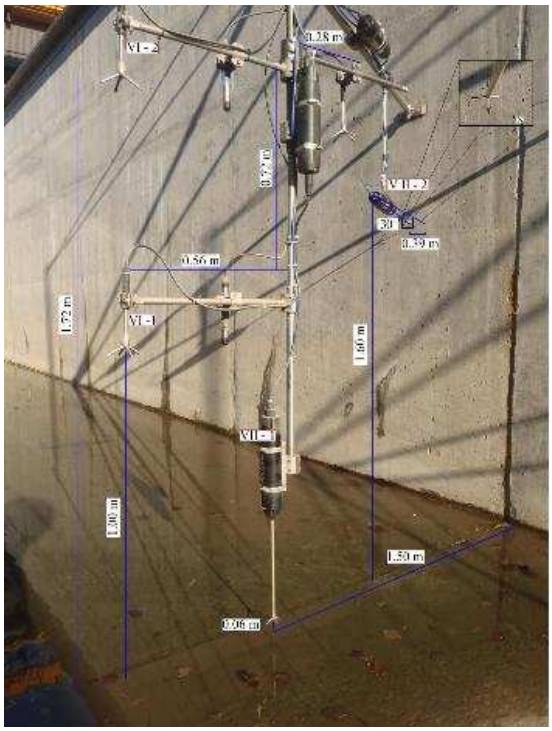

Figure 4. Experimental set-up at station 1. Two Vectrino current meters (VI) and two water level probes (WG) were positioned at 1.00 m and 1.70 m above the bottom, one Vectrino II current meter (VII-1) was positioned at 6 cm above the concrete floor and a second Vectrino II (VII-2) was positioned at 0.39 cm from the concrete wall to quantify wall-induced turbulence.

Each station was equipped with 2 water level probes to monitor water level fluctuations, 2 ADV Vectrino current meters to measure water velocity within the water column in three dimensions and 2 ADV Vectrino II current meters to quantify wall- and floor-induced turbulence (Fig. 4). The *x* axis was oriented along the wave propagation direction (*u*-velocity component); the *y* axis was oriented to the left wall (*y*-velocity component); and the *z* axis, was orientated toward the water surface *(w*-velocity component). Each of the ADV measuring probes used in the experiments consisted of a down-looking acoustic transmitting sensor mounted on a stem (36 cm long and 7 mm diameter), and surrounded by three equi-spaced receiving transducers.

The ADV Vectrino II profiles the water column over a 3 cm range and provides three-component velocity observations with a resolution as fine as 1 mm and sampling rate as fast as 100 Hz. This enables the measurements to be made in near-bed region without interfering with the flow. For this set of tests, water level probes and Vectrino current meter probes were positioned respectively at 100 cm and 170 cm above the floor and at 157 cm and 206 cm from the left side wall at stations 1 and 3, at 77 cm and 167 cm above the floor and at 159 cm and 222 cm from the left side wall at station 5, and at 77 cm and 130 cm above the floor and at 159 cm and 143 cm from the left side wall at station 7 (Fig. 3). The two ADV Vectrino II were positioned respectively at 6.5 cm above the concrete floor and at 3.9 cm from the left wall to collect velocity profiles at a rate of 10 Hz. Vectrino II current meters were mounted only at stations 1 and 2. In parallel, 5 capacitance sensors were fixed at 45 m, 55 m, 65 m, 75 m and 85 m on the right side wall, to record wave profile during its progression in the flume and quantify potential wave deformation.

3. Results

3.1. *Flow structure*

The flow structure was quantified using the instantaneous and time-averaged velocity vector components (respectively (*u*, *y*, *w*) and ($\hat{u}$, $\hat{y}$, $\hat{w}$)), the primary Reynolds stresses -*u'w'* and -*y'w'*, and the transverse

Reynolds stress $-u'y'$, where u', y' and w' are the velocity vector components variations. Results indicate that, for small wave amplitude ($H \leq 1.0$ m), instantaneous longitudinal velocity u ranges from -45 cm/s to 30cm/s, instantaneous transversal velocity y ranges from -10 cm/s to 10 cm/s and instantaneous vertical velocity w ranges from -35 cm/s to 35 cm/s (Fig. 5). Mean water particle velocities range from 0 cm/s to -4 cm/s for $\hat{u}$ and $\hat{y}$, and from 0 cm/s to 2 cm/s in $\hat{w}$, indicating the existence of a small net water mass transport oriented from the end of the flume to the wave maker. Mean primary Reynolds stress ranges respectively between 0 cm²/s² and 1.2 cm²/s², while the mean transverse Reynolds stress ranges between 0 cm²/s² and 0.5 cm²/s².

For greater wave amplitude ($1.0 < H \leq 1.5$ m), instantaneous longitudinal velocity u ranges from -110 cm/s to 130 cm/s instantaneous transversal velocity y ranges from -20 cm/s to 20 cm/s and instantaneous vertical velocity w ranges from -45 cm/s to 45 cm/s. Mean water particle velocities range from -10 cm/s to -30 cm/s for $\hat{u}$, from -1 cm/s to 6 cm/s for $\hat{y}$ and from 0 cm/s to 5 cm/s for $\hat{w}$. Mean primary Reynolds stress ranges respectively between 0.2 cm²/s² and 7.6 cm²/s² while the mean transverse Reynolds stress ranges between 0.1 cm²/s² and 0.6 cm²/s².

Above the concrete floor, current velocities measured by ADV Vectrino II reveal the existence of a turbulent layer of a few centimeters of thickness where turbulent eddies are present and instantaneous velocity variations can reach locally 1 m/s (Fig. 6). For a water depth of 2.5 m, the turbulent layer is not observable for very short wave periods ($T \leq 1.5$ s). For longer wave periods, the layer thickness increases rapidly to 1.7 cm. However, turbulent eddies appear occasionally higher above the concrete floor, in a layer located between 2.6 cm and 3.5 cm above the floor (Fig. 6). For a water depth of 3.0 m and small wave amplitude ($H = 0.5$ m), the turbulent layer doesn't develop for any of the tested wave periods (from 1.5 s to 10 s). For higher wave height ($H = 1.0$ m), a turbulent bottom layer appears for wave period of 10 seconds or higher. The layer thickness remains however relatively small (0.6 cm). For wave height of 1.5 m, a 0.1 cm thick turbulent layer appears for a 6 seconds wave period, increasing to 1.3 cm for wave period of 8 seconds and higher.

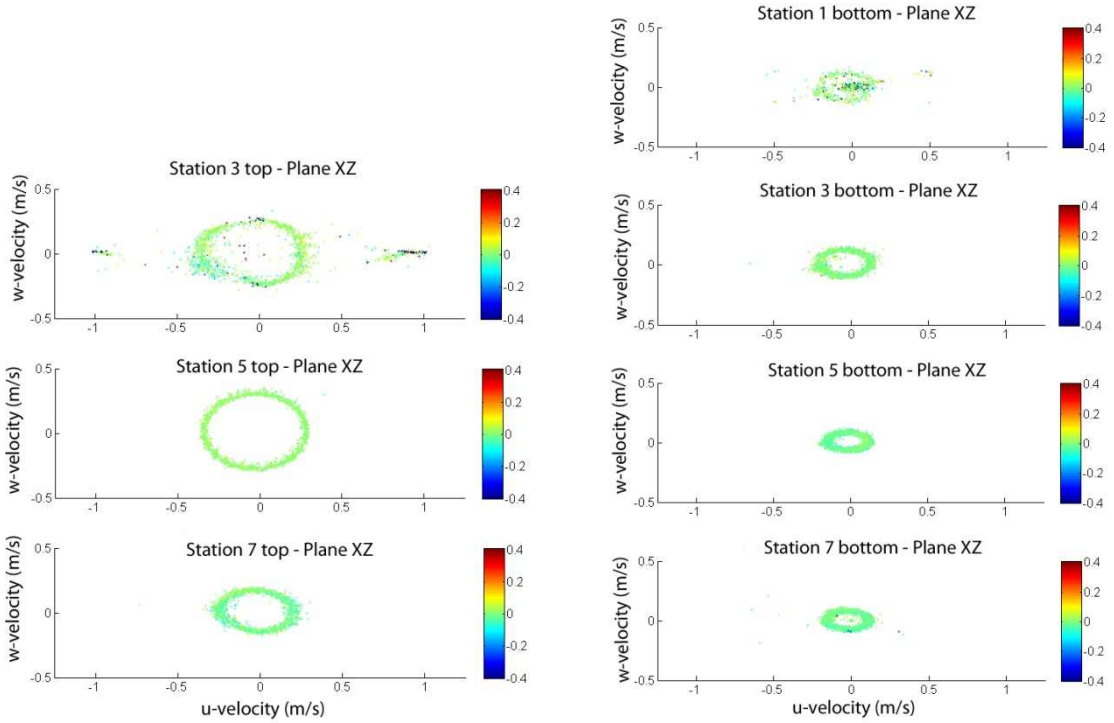

Figure 5. Velocity plot of the components u, y and w for each station (1, 3, 5 and 7) for $H = 0.5$ m, $T = 2$s and $h = 2.5$ m. Colors represent the y velocity component. All velocities are in m/s.

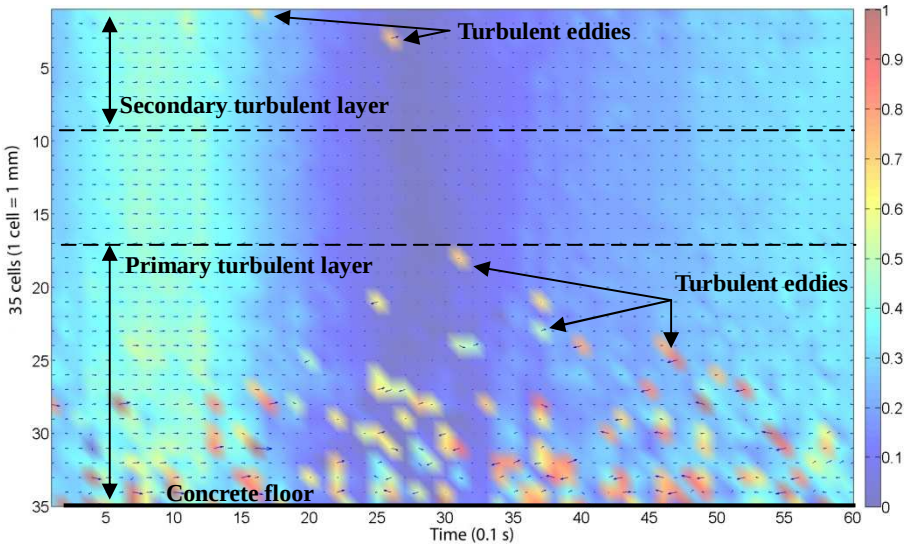

Figure 6. Velocity vectors measured by ADV Vectrino II in a 3.5 cm water column located above the concrete floor of the flume. Measurements were acquired at station 3 for H = 0.5 m, T = 8 s and h = 2.5 m.

3.2. *Wave analysis*

Water level was recorded by water gages and compared with the theoretical simulated wave shape (Airy wave or sine wave). Figure 7 show the results for a mean water level of 2.5 m and a wave height of 0.5 m. The measured wave amplitude is significantly smaller than expected for short wave periods, with a difference of –16.5 cm for T = 1.5 s, –3 cm for T =2 s, and –10 cm for T = 4s. For longer wave periods, the discrepancy between the theoretical sine wave amplitude and the measured wave amplitude is smaller. The mean difference is only –6 cm for T = 6 s, –4 cm for T= 8 s and –5 cm for T = 10 s. The wave shape is also altered by bed friction for longer wave periods and tends to a cnoidal shape with steeper crests and flatter troughs. For higher wave height (H = 1.0 m, Fig. 9), the discrepancy between measured wave amplitude and theoretical wave amplitude increases significantly with a mean difference of –40 cm for T = 2 s and –30 cm for T = 4 s. For longer wave periods, the wave amplitude difference is smaller with –10 cm for T = 6 s, –5 cm for T = 8 s and 0 cm for T = 10 s. The cnoidal shape is also more pronounced and secondary waves with lower amplitude are added to the dominant waves (Fig. 9).

Spectral analysis was performed on the water level records using a Fast Fourier Transform (FFT). Results indicate that wave energy is not concentrated on a single peak but is distributed on multiple peaks corresponding to higher harmonics of the cnoidal wave shape. The two main spectral energy peaks correspond to the fundamental wave frequency f_1 and to the second order harmonic frequency $f_2 = 2f_1$ (Fig. 8 and 10). For short wave periods ($T \leq 4$ s), the spectral energy density for the 2nd order harmonic f_2 is small compared to the spectral energy density for the fundamental frequency f_1 (less than 15% of the fundamental wave energy for H= 0.5 m, and less than 3% of the fundamental wave energy for H = 1.0 m).

However, for longer wave periods (T > 4 s), spectral energy density for f_2 increases and reaches 50% of the fundamental wave energy for T = 10 s (f_1 = 0.1 Hz) and H = 0.5 m. When H = 1.0 m, the spectral energy density for f_2 represents 75 % of the dominant wave energy for T = 10 s (f_1 = 0.1 Hz). Moreover, the spectral analysis indicates that, for long wave periods ($T \geq 8$ s or $f_1 \leq 0.17$ Hz), energy density increases in third and fourth order harmonics $f_3 = 3f_1$ and $f_4 = 4f_1$. For a 10 seconds wave period and 0.5 m wave height, the spectral energy density for f_3 and f_4 is respectively 48% and 24% of the fundamental wave energy. For a 10 seconds wave period and 1.0 m wave height, the spectral energy density for f_3 and f_4 increases respectively to 54% and 31% of the fundamental wave energy.

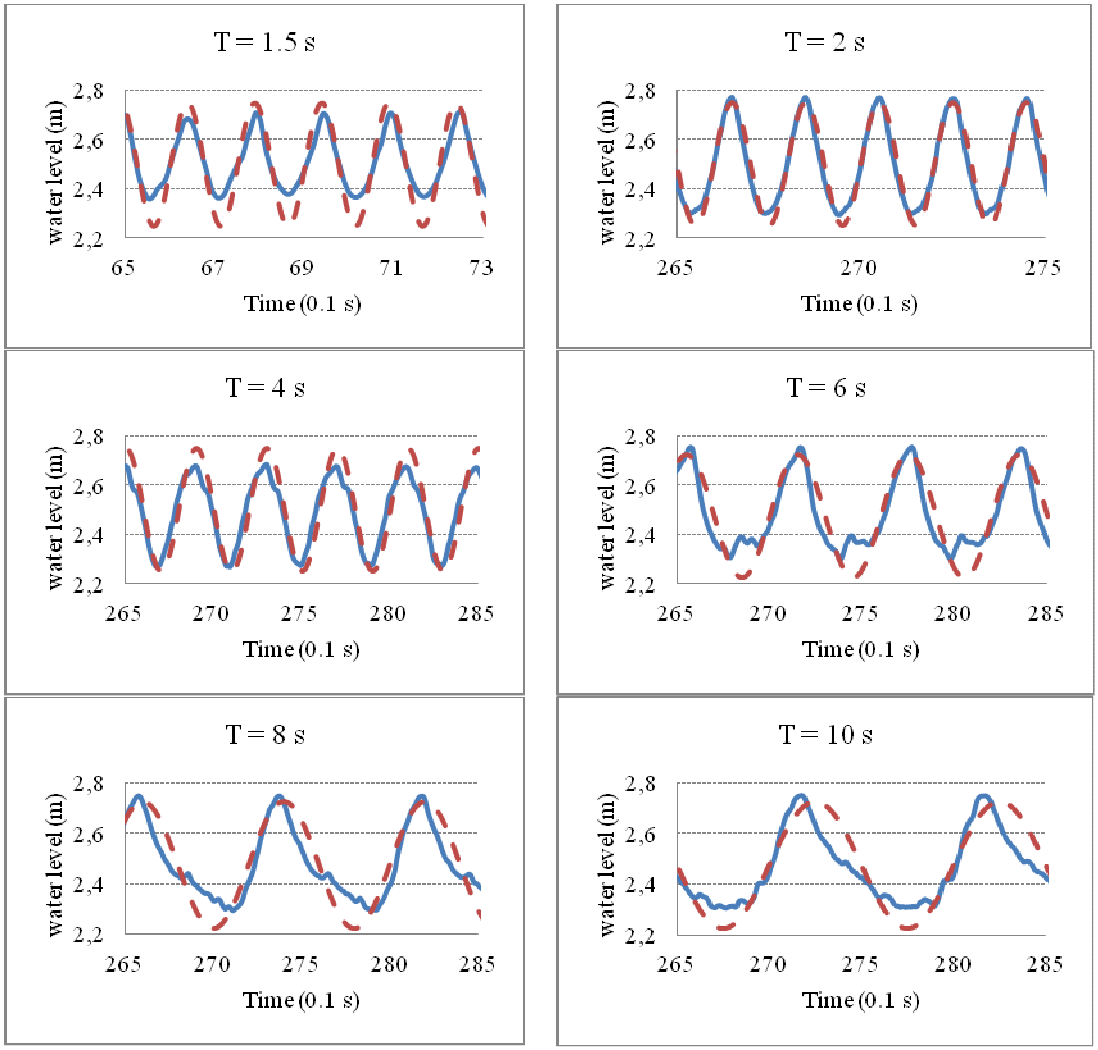

Figure 7. Wave shape recorded (blue line) in function of wave period T for h = 2.5 m and H = 0.5 m. Red dotted line is the theoretical wave shape of the simulated wave (sine wave).

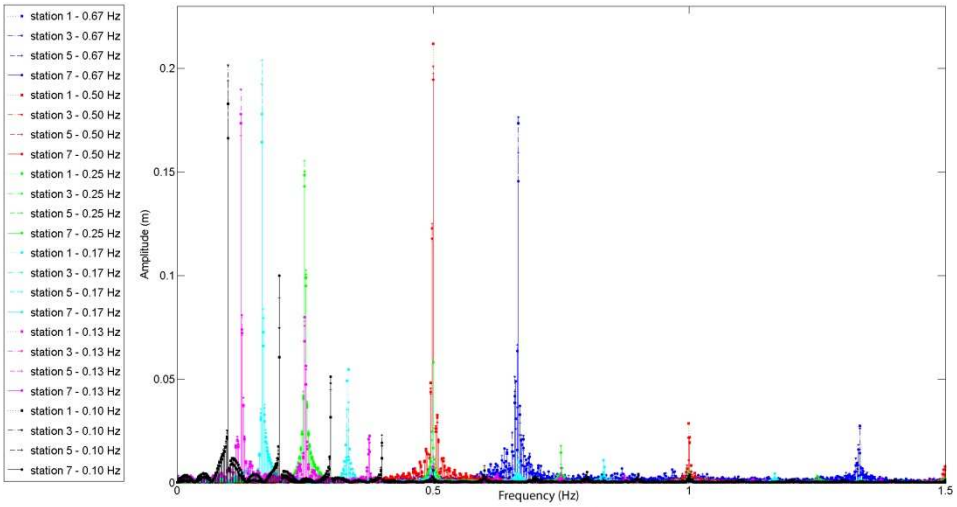

Figure 8. Spectral analysis for h = 2.5 m and H = 0.5 m. Secondary energy peaks are observables for sub frequencies $f_2 = 2f_1$ (or $T_2 = T_1/2$).

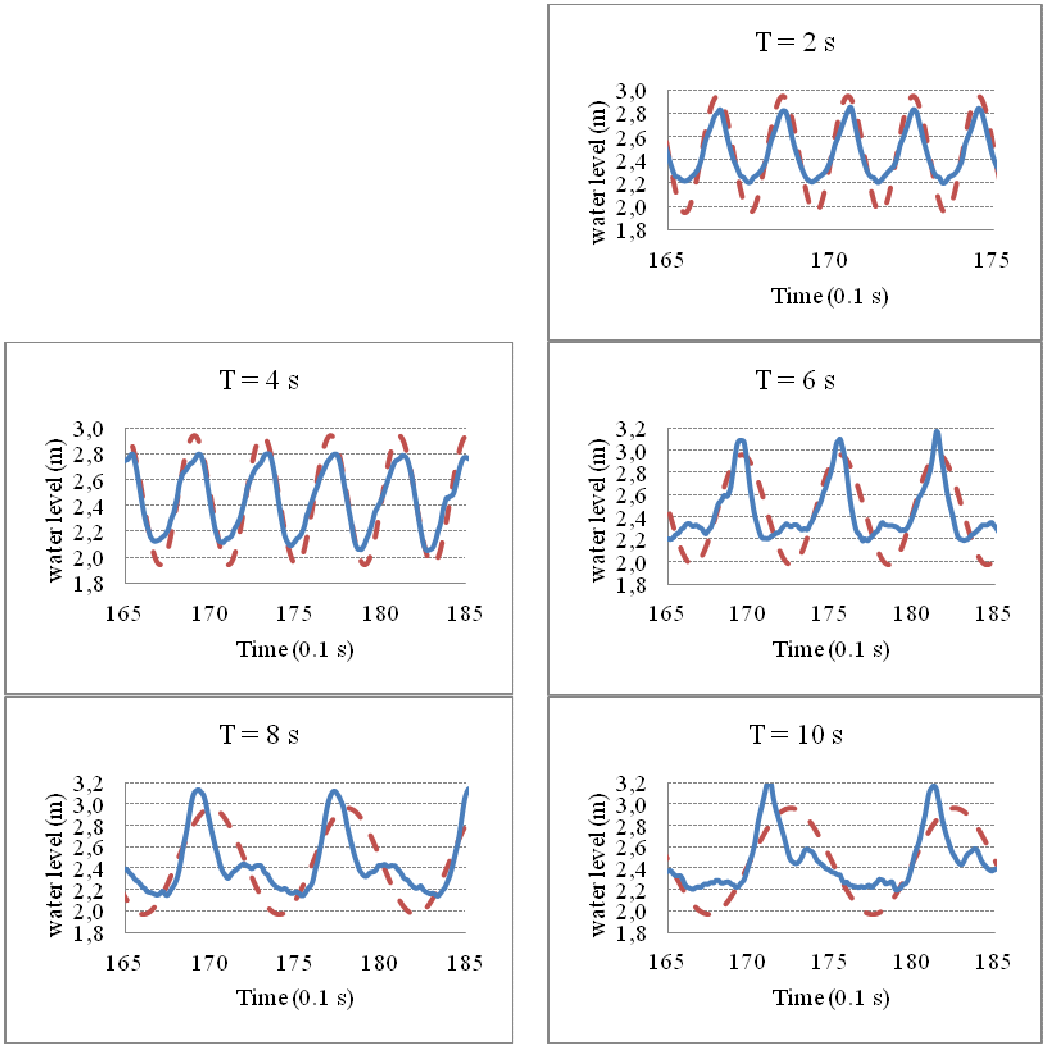

Figure 9. Wave shape recorded (blue line) in function of wave period T for h = 2.5 m and H = 1.0 m. Red dotted line is the theoretical wave shape of the simulated wave (sine wave).

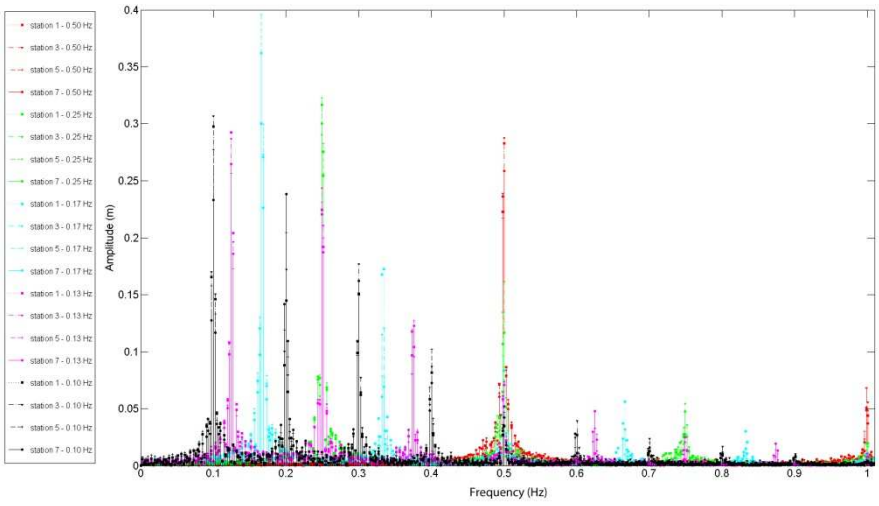

Figure 10. Spectral analysis for h = 2.5 m and H = 1.0 m. Secondary energy peaks are observables for sub frequencies $f_2 = 2f_1$ (or $T_2 = T_1/2$).

4. Discussion

ADV Vectrino current meters reveal the existence of a significant water flow that takes place within the water column under sine wave conditions. ADV measurements indicate that the flow is oriented in the opposite direction of wave propagation, from the end of the flume to the wave maker, and can be assimilated to a undertow current. The observed return flow velocity is relatively small for small wave amplitude (H = 0.5 m) with a time-averaged *u*-velocity component of only -4 cm/s. But flow velocity can reach -30 cm/s for wave height of 1.5 m. The existence of a return flow under progressive, non breaking sine waves has already been observed in other flume experiments (Fig. 11) by several authors (i.e. Klopman, 1994; Fredsøe et al., 1999). As the end of the flume prohibits net flow of water, a hydraulic flume can be described as a zero net flow system. In Eulerian terms, the horizontal particle velocity at a fixed point under sine waves has the form:

$$u(x,z,t) = \bar{u}(z)\cos\omega t \tag{1}$$

and the mean horizontal velocity $\bar{U}(x,z,t)= 0$ for all points. However, this is only true below the wave trough where there is water at all times. At levels between the trough and the crest, the water surface goes below during a given time interval, resulting in a positive net flow rate *Q* above the trough which can be expressed as (Nielsen, 2009):

$$Q = \int_{-H/2}^{H/2}\int_{t_u(z)}^{t_d(z)} u(z)\cos\omega t\, dt\, dz \approx \overline{\eta u(x,0,t)} = \frac{gH^2}{8c} \tag{2}$$

As net flow of water is prevented by the end wall of the flume, this net flow rate leads to a slight water accumulation at the end of the flume, which in turn, drives a steady return flow so that the net flow of water in the flume remains equal to zero (Nielsen, 2009).

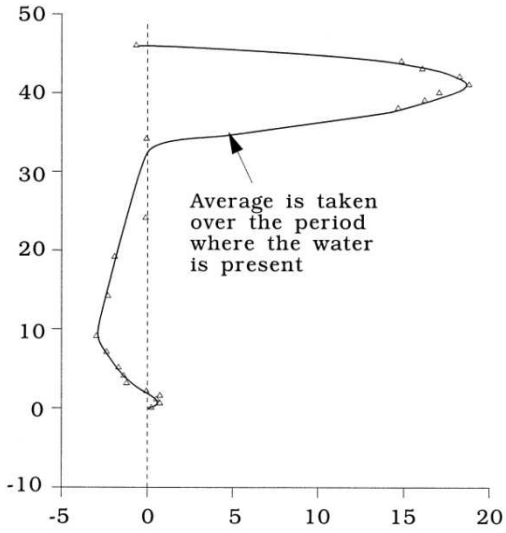

Figure 11. Eulerian period-averaged velocities in a zero net flow situation (Fredsøe et al., 1999).

ADV results also indicate the existence of a turbulent layer above the concrete floor of the flume where turbulent eddies are observed. The layer thickness ranges between 1.3 cm and 1.7 cm depending of wave height. ADV Vectrino II velocity profiles also reveal the presence of turbulent eddies upper in the water column, between 2.6 cm and 3.5 cm above the concrete floor. This secondary turbulent layer is not present all the time and doesn't seem to be related to bed friction. It is rather interpreted as turbulence induced by the ADV probe or the monitoring station framework.

Wave amplitude discrepancies between water level records and theoretical sine wave have highlighted a problem with the monitoring software that controls the wave maker. This bug has been corrected and future tests are planned to confirm the correction of this problem. However, wave records analysis also

shows that wave shape can be greatly modified during its propagation in the flume. For wave period $T \leq 2$ s, the flume can be considered as a "deep water" environment. Sine waves propagate without deformation and Airy theory can be applied to describe their propagation. For wave period $2 \text{ s} < T \leq 6$ s, the flume should be considered as a "transitional" environment. Sine waves begin to be deformed by bed friction and non-linear shallow water equations should be considered to describe wave shape and wave propagation. Depending on *L/h* ratio, the Stokes solution or the cnoidal solution would be used. For higher wave period ($T > 6$ s), the flume should be considered as a "shallow water" environment. Sine waves are significantly deformed and cnoidal wave theory has to be used to describe their shape and propagation characteristics.

5. Conclusion

In this paper, the design of the new Quebec long flume was presented and the preliminary results of the first hydraulic tests were discussed. Results indicate that, under progressive, non breaking sine waves, the floor-induced turbulence is limited to a narrow layer of only 1.7 cm above the concrete floor. A significant return flow, oriented in the opposite direction of wave propagation, was also detected under sine waves. Measured mean horizontal velocities for this return flow range between -4 cm/s and -30 cm/s depending on the wave height. Water level was also recorded by water gages and compared with the theoretical simulated wave shape (Airy wave or sine wave). Preliminary results showed that the wave shape is altered by bed friction for long wave periods ($T \geq 6$ s) and tends to a cnoidal shape with steeper crests and flatter troughs. These findings will allow correcting systematic flume-induced biases and will lead to more accurate measurements in forthcoming hydraulics experiments.

Acknowledgements

This project was funded by the Government of Canada and the Government of Quebec. The authors would also like to thank Louis-Frédéric Daigle, Corinne Brunelle and Constant Pilote for their contribution to this study.

References

Baltsavias, E.P. 1999. A comparison between photogrammetry and laser scanning. *ISPRS Journal of Photogrammetry & Remote Sensing*, 54: 83-94.

Brock, J.C., Wright, C.W., Sallenger, A.H., Krabill, W.B., and Swift, R.N., 2002. Basis and methods of NASA airborne topographic mapper Lidar surveys for coastal studies. *Journal of Coastal Research*, 18(1): 1-13.

Dalrymple, R.A., 1989. Physical modeling of littoral processes, in *Recent Advances In Hydraulic Physical Modelling*, R. Martins, Ed., Kluwer Academic Publishers, Dordrecht, The Netherlands, 567-588.

Dette, H.H., Larson, M., Murphy, J., Newe, J., Peters, K., Reniers, A., Steetzel, H., 2002. Application of prototype flum e tests for beach nourishment assessment. *Coastal Engineering*, 47: 137- 177.

Fenton, J. D., 1990. Nonlinear wave theories, in *The Sea - Ocean Engineering Science*, B. Le Méhauté & D. M. Hanes (Eds), Wiley, New York, 9: 1–25.

Fredsøe, J., Andersen, K.H., Mutlu Sumer, B., 1999. Wave plus current over a ripple-covered bed. *Coastal Engineering*, 38: 177-221.

Hasselmann, K., Ross, D.B., Muller, P., Sell, W., 1976. Parametric wave prediction model. *Journal of Physical Oceanography*, 6: 200–228.

Heller, V., 2011. Scale effects in physical hydraulic engineering models. *Journal of Hydraulic Research*, 49(3): 293-306.

Hudson, R.Y., Herrmann, F.A., Sager, R.A., Whalin, R.W., Keulegan, G.H., Chatham, C.E., Hales, L.Z., 1979. *Coastal Hydraulic Models*, special report n° 5, US Army Engineer Waterways Experiment Station, Vicksburg, Mississippi, USA.

Hughes, S.A., 1993. *Physical Models and Laboratory Techniques In Coastal Engineering*, World Scientific Publishing, London.

Irish, J.L., McClung, J.K. and Lillycrop, W.J., 2000. Airborne lidar bathymetry: the SHOALS system. *PIANC Bulletin*, 2000, 103: 43-53.

Kamphuis, J.W., 1974. Practical scaling of coastal models. *Proceedings of the 14th Coastal Engineering Conference, A merican Society of Civil Engineers*, 3: 2086-2101.

Klopman, G., 1994. Vertical structure of the flow due to waves and currents. *Delft Hydraulics Progress Report H840.30 Part II*.

Krabill, W.B., Thomas, R.H., Martin, C.F., Swift, R.N., and Frederick, E.B., 1995. Accuracy of airborne laser altimetry over the Greenland ice sheet. *Int. J. Remote Sensing*, 16: 1211-1222.

Long, B.F., and Robitaille, V., 2009. Use of a multi-beam autonomous portable laser equipment (MAPLE) to measure t he reflectance of shallow water facies and habitats - a new tool to calibrate airborne laser bathymetry instruments. *Proceedings of the 2nd FUDOTERAM Workshop*, Québec, Canada.

Long, B.F., Aucoin, F., Montreuil, S., Robitaille, V., Xhardé, R., 2010. Airborne LiDAR bathymetry applied to coastal hydrodynamic processes. *Coastal Engineering Proceedings*, 1(32), sediment.26. doi:10.9753/icce.v32.sediment.26

Nielsen, P., 2009. *Coastal and Estuarine Processes*. World Scientific Publishing, London.

Ochi, M.K., Hubble, E.N., 1976. On six-parameter wave spectra. *Proceedings of the 15th International Conference on Coastal Engineering*, Honolulu, Hawaii , 301–328.

Pierson, W.J., Moskowitz, L., 1964. A proposed spectral form for fully developed wind seas based on the similarity theory of S.A. Kitaigorodskii. *Journal of Geophysical Research*, 69: 5181–5190.

Svendsen, I.A., Jonsson, I.G., 1976. *Hydrodynamics of Coastal Regions*. Den Private Ingenioerfond, Lyngby.